52 V

Journal of Sound and Vibration (1992) **154**(1), 45–66

EMPIRICAL FLUID-ELASTIC MODELS AND CHAOTIC GALLOPING: A CASE STUDY

E. SIMIU AND G. R. COOK

Building and Fire Research Laboratory, National Institute of Standards and Technology, Gaithersburg, Maryland 20899, *U.S.A.*

(*Received* 1 *November* 1990 *and in final form* 15 *February* 1991)

To describe the behavior of bluff body fluid-elastic motions, analysts must in practice resort to empirical models based on a limited number of measured fluid-elastic behavior characteristics. To our knowledge the question of whether such models can predict reliably the actual occurrence of chaos has not yet been addressed. With a view to answering this question in a specific case, we present an exploratory experimental and numerical study of two paradigmatic fluid-elastic systems: (1) a single galloping square prism; and (2) a pair of elastically coupled galloping prisms which can exhibit apparently chaotic behavior of interest from a structural engineering viewpoint. We review various conventional empirical models and their capabilities, and develop a model that incorporates information on the dependence on angle of attack of the vortex-induced lift coefficient and the Strouhal number for the stationary prism. For appropriate values of the adjustable parameters and initial conditions, this model appears to be able to describe observed behavior at least qualitatively. However, the predictive capabilities of the model are poor, especially for apparently chaotic behavior. A possible approach to improving the reliability of the numerical detection of such behavior is suggested.

1. INTRODUCTION

Experience shows that as novel, increasingly daring types of structures emerge, they may be affected by unsuspected forms of undesirable behavior. Cast iron column buckling before Euler and suspension bridge flutter 50 years ago are cases in point. As compliant structures are built in increasingly deeper waters and exhibit increasingly strong nonlinearities, there is concern that they may be affected by undesirable fluid-elastic behavior, including chaotic behavior [1–3]. Thus recent progress in dynamical systems theory has stimulated interest in the chaotic behavior of compliant offshore structures, or elements thereof, and of other fluid-elastic systems [3–8].

In offshore structures the oscillating bodies are bluff, and if flow separation effects are significant the fluid-elastic loads can seldom in practice be obtained by solving the Navier–Stokes equations. For this reason the analyst is forced to resort to empirical models. Chaotic dynamics studies of bluff body fluid-elastic systems quoted earlier do not include comparisons between results of empirical modeling and experiment. Thus, the question of whether empirical fluid-elastic models can predict reliably the actual occurrence of motions that are or appear to be chaotic remains open.

The purpose of this paper is to address this question in a specific case. To this end we conducted an exploratory experimental and numerical study of the two simple bluff body fluid-elastic systems shown in Figure 1, referred to for brevity as the single and the double oscillator. The systems were chosen on account of their interesting dynamic behavior, of their relative simplicity compared to the well-known case of the circular cylinder (from

0022-460X/92/070045+22 $03.00/0

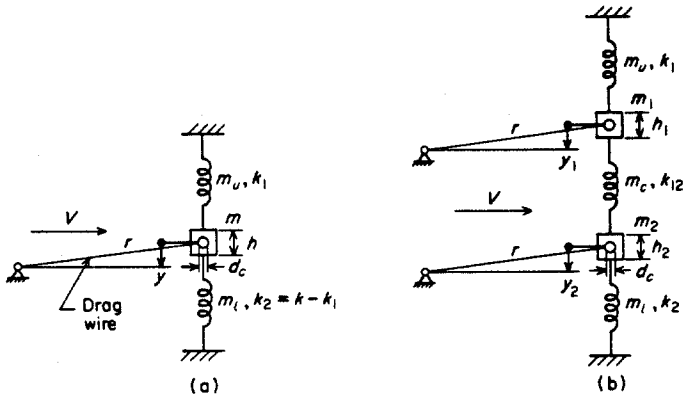

Figure 1. Schematic of (a) single oscillator and (b) double oscillator.

which they differ by having fixed separation points), and of the relative ease and low cost of their physical testing. In both systems the prisms experience galloping and vortex-induced oscillations transverse to the mean flow. We describe the experimental set-up and present typical experimental results. In the case of the double oscillator these results reveal an interesting form of apparently chaotic fluid-elastic behavior. We then address the modeling issue. The equations of motion for the single oscillator are presented first. We then review briefly empirical fluid-elastic models proposed in the literature [10–17] and assess them in the light of our experimental results. We develop an alternative model which accounts for the dependence on angle of attack of the Strouhal number and the vortex-induced lift for the stationary prism, and thus makes it possible naturally to couple the equation of motion of the prism and the lift oscillator equation yielding the vortex-induced lift. We assess the performance of our fluid-elastic model in the single oscillator case. We then present the equations of motion for the double oscillator, apply our fluid-elastic model in this case, and comment on its descriptive and predictive capabilities.

2. DESCRIPTION OF EXPERIMENTS

The experiments were performed in the 12 in (0·3048 m) diameter water tunnel of the David Taylor Research Center, Bethesda, Maryland (Figure 2). The square prisms were tested at about 0·3 m downstream from the entrance nozzle. At that location the flow is uniform (with turbulence intensity of approximately 1–2%) over a 0·32 m diameter circular area concentric with the nozzle. The nominal flow speed readings were calibrated using

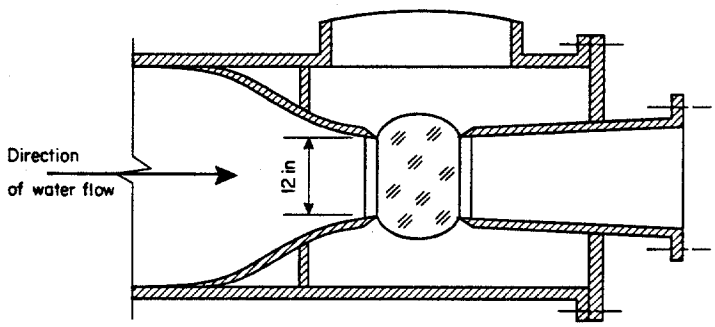

Figure 2. Schematic longitudinal cross-section of test chamber.

measurements with the experimental device in place. Within a few centimeters outside of the uniform flow area the flow within the test chamber is approximately quiescent. The single oscillator prism was placed at the center of the circular area. For the double oscillator the distance between the axis of each prism and the center of the circular area was about 50 mm. The prisms were made of solid steel or solid aluminium. Their sides and lengths were: for prism 1 (steel), $h=6{\cdot}35$ mm, $L=215$ mm; for prism 2 (aluminium), $h=6{\cdot}35$ mm, $L=230$ mm; and for prism 3 (aluminium), $h=12{\cdot}7$ mm, $L=215$ mm.

Plastic 20 mm diameter, 1/4 mm thick end plates were fitted to the prisms. Threaded steel rods with diameter $d_c=2$ mm and a clear length $L_c=60$ mm were screwed into the centers of the end faces of the prisms. The springs were connected by small aluminium connectors to these rods, and were thus located within the approximately quiescent zone of the test chamber. Gage 28 ($d_w=0{\cdot}328$ mm diameter) brass drag wires with length $r=400$ mm were used to tie the 2 mm rods to screws protruding from adjustable brackets. The drag wires moved in vertical planes at all times and were nearly horizontal when the prisms were at rest (Figure 1). Measurements showed that the damping ratio in air was $\beta_{air}\simeq 0{\cdot}005\%$. The total mass of one prism and its appurtenances was 0·074 kg for the steel prism with 6·35 mm sides, 0·033 kg for the aluminium prism with 6·35 mm sides, and 0·101 kg for the aluminium prism with 12·7 mm sides. Time histories of the motion were obtained by connecting the fixed ends of the top and bottom springs to cantilevered aluminium bars provided with strain gages. Data were acquired at a 500/s sampling rate.

3. TYPICAL EXPERIMENTAL RESULTS

3.1. SINGLE OSCILLATOR

Typical displacement time histories for the single oscillator are shown in Figure 3 (aluminium bar, $h=12{\cdot}7$ mm, total spring constant $k=127$ N/m, upper spring mass $m_u=14$ g, lower spring mass $m_l=14$ g, flow speeds $V=0{\cdot}92$ m/s (a) and $V=2{\cdot}62$ m/s (b), respectively) and Figure 4, (steel bar, $h=6{\cdot}35$ mm, $k=70$ N/m, $m_u=5$ g, $m_l=5$ g, $V=0{\cdot}91$ m/s (a) and $V=1{\cdot}77$ m/s (b), respectively). All observed motions, including those of Figures 3 and 4, exhibited amplitude modulation.

3.2. DOUBLE OSCILLATOR

Typical displacement-time histories for the double oscillator are shown in Figures 5(a, b, c) (aluminium bars, $h=6{\cdot}35$ mm, top spring constant $k_1=56$ N/m, lower spring constant $k_2=78$ N/m, coupling spring constant $k_{12}=145$ N/m, $m_u=10$ g, $m_l=7$ g, $m_c=4$ g, $V=0{\cdot}91$ m/s, $V=1{\cdot}34$ m/s and $V=1{\cdot}77$ m/s, respectively). For clarity we show in Figures 5(a, b, c) only the motions of the top prism. In Figure 5(d) are shown the motions of both the top and the bottom prisms for a 5 s interval of Figure 5(c).

In Figure 5(a) the top and bottom prisms oscillate in phase at all times. This is typical and velocities lower than a critical velocity V_{ce}. Column 7 of Table 1 shows the observed values V_{ce} corresponding to various sets of system parameters. Note that for cases 1 and 2 the ratios $(k_i)_1/(k_i)_2$ $(i=1, 2, 12)$ and the respective masses, m, are approximately the same. Therefore, as required by similarity, so are the respective non-dimensional ratios $V_{ce}/[h(k_i/m)^{1/2}]$.

Figures 5(b, c) are typical of oscillations occurring for $V>V_{ce}$: two oscillatory forms alternate spontaneously, one in which the two prisms move in phase, the other in which they move in opposite phases (Figure 5(d)). These motions are reminiscent of the irregular alternation among different oscillatory forms in the chaotic motion of the forced buckled column (i.e., the alternation among oscillations about the stable fixed points and the unstable fixed point of the unforced column) [21, 22]. The motions are highly irregular,

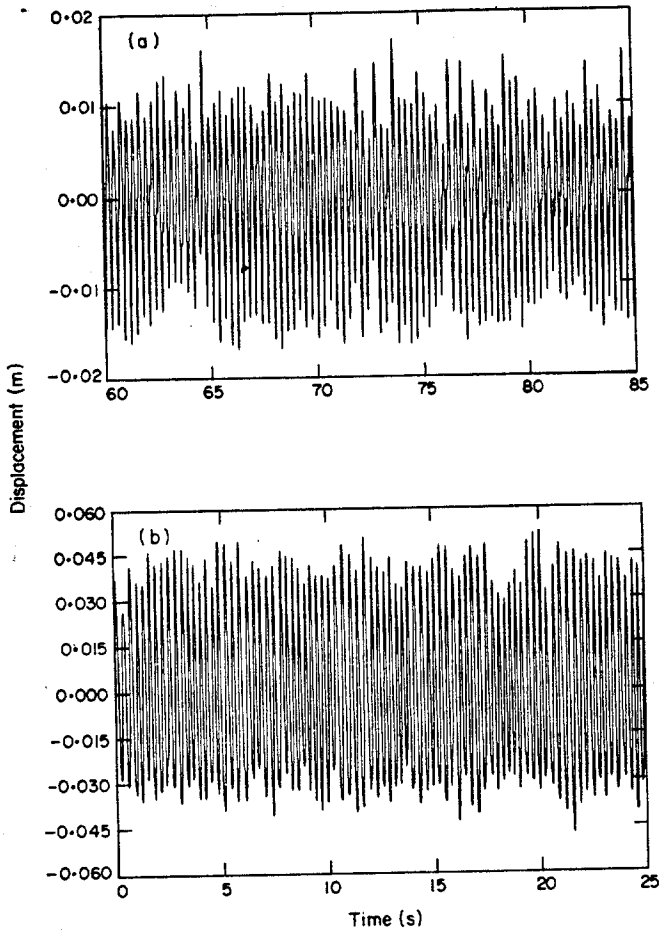

Figure 3. Observed response of single aluminium prism ($h=0{\cdot}0127$ m, aluminium): (a) $V=0{\cdot}92$ m/s; (b) $V=2{\cdot}62$ m/s.

and for any given system the average interval between successive alternations decreases as the flow velocity increases. To characterize the motions we considered Poincaré plots obtained by intersecting the orbit with the surface of section $\dot{y}_1=0$, $\ddot{y}_1<0$, where $\dot{y}_1$ is the velocity of the top prism. These plots map maximum displacements of the top prism *vs.* their immediate antecedents. If the motion was periodic with n local maxima per period, or if it was quasi-periodic, the Poincaré plots would consist, respectively, of n points or of a dense set of points on a curve (surrounded in both cases by small clouds due to noise). Instead, as shown typically by Figure 6, which corresponds to the record partially depicted in Figure 5(c), points are spread out in large clouds (except for those lying near the bisector, which represent nearly equal successive displacement maxima, e.g., maxima near $t=86$ s and $t=88$ s in Figure 5(c)). This suggests that the motions are neither periodic nor quasi-periodic. We also found that the spectral density functions for these motions contain significantly higher broadband components than motions such as those of Figure 5(a). Motions such as those of Figures 5(b, c) thus appear to be chaotic, a point to be further discussed subsequently.

Fractal dimension calculations applied to the experimental data would be useful for confirming this assumption [18]. Unfortunately, as is the case for Lyapounov exponents

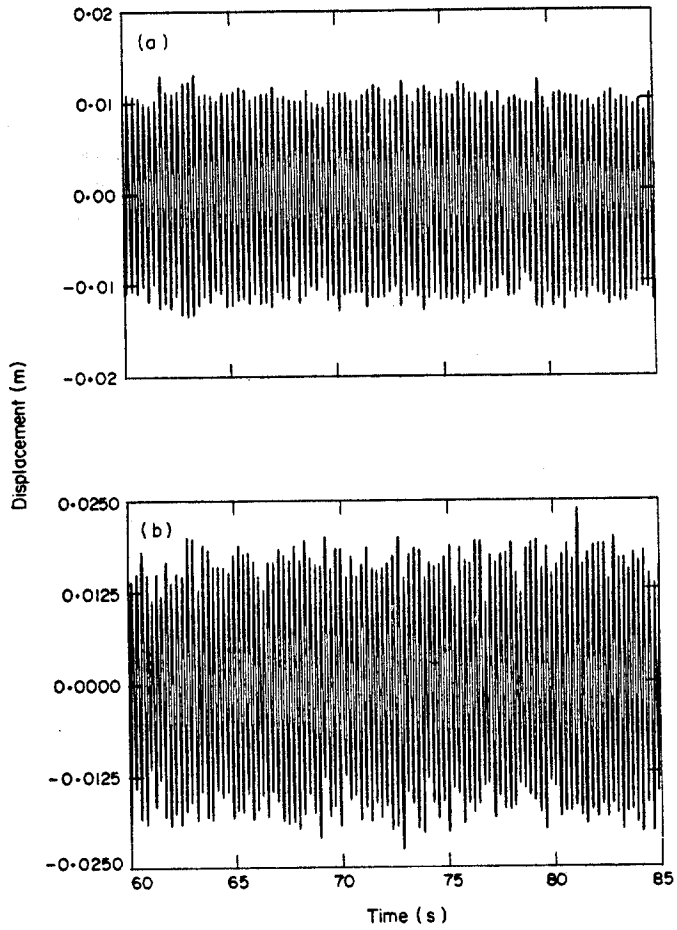

Figure 4. Observed response of single prism ($h=0{\cdot}00635$ m, steel): (a) $V=0{\cdot}91$ m/s; (b) $V=1{\cdot}77$ m/s.

[19], it appears that at present such calculations cannot be performed with confidence for experimental systems with, say, eight or more phase space dimensions, see, e.g., reference [20, p. 13].

3.3. FLOW VISUALIZATION

The wake flow was visualized by using a 4 W vertical laser light sheet passing through the mid-span of the galloping bars. Fluorescein dye was pumped from a reservoir through feed tubes which released the dye near the light sheet at the mid-height of the upstream faces of the prisms. A high-speed video tape recorder was used to record images of up to 250 frames per second. For the double oscillator the image of the wake tends to be less clear for the lower prism owing to flow pollution by the dye. In addition, the upper prism casts a shadow on to the wake of the lower prism.

In Figure 7 (aluminium bars, $h=6{\cdot}35$ mm, $k_1=53$ N/m, $k_2=61$ N/m, $k_{12}=80$ N/m, $m_u=7$ g, $m_l=6$ g, $m_c=5$ g and $V=0{\cdot}85$ m/s) are shown typical visualizations of the wake of the upper prism at successive intervals of duration $15/250=0{\cdot}06$ s, equal to the average interval between the shedding of successive vortices. The vortex shedding frequency, n_s, appears to be approximately independent of the oscillatory motion and of whether or not

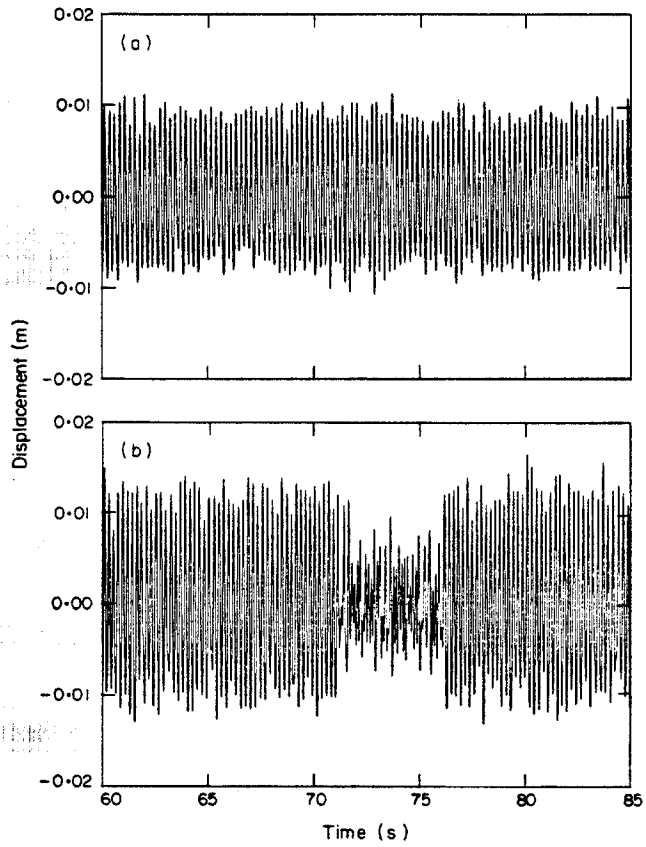

Figure 5. Observed response, double oscillator ($h_1 = h_2 = 0{\cdot}00635$ m, aluminium prisms): (a) top prism, $V = 0{\cdot}91$ m/s; (b) top prism, $V = 1{\cdot}34$ m/s; (c) top prism, $V = 1{\cdot}77$ m/s; (d) top prism (solid line), bottom prism (dotted line), $V = 1{\cdot}77$ m/s.

alternation between oscillatory forms occurs. Since

$$n_s = SV/h, \tag{1}$$

where S is the Strouhal number, Figure 7 is approximately consistent with an average value $S \simeq 0{\cdot}00635/0{\cdot}060/0{\cdot}85 \simeq 0{\cdot}1245$, *vs.* 0·125, as reported in references [30, 31]. Flow visualizations for the single oscillator yielded similar results.

In Figure 8 are shown typical wakes of the upper and lower prism for the same set-up as in Figure 7, suggesting that the vortex shedding in the wake of the two prisms occurs either approximately in phase (Figure 8(a)) or in approximately opposite phases (Figure 8(b)).

4. EQUATION OF MOTION FOR SINGLE OSCILLATOR

For the single oscillator of Figure 1(a), the equation of motion is written as

$$D(y) \equiv m\ddot{y} + c\dot{y} + k_r y + \tfrac{1}{2}\rho C_d A \dot{y}|\dot{y}| - \tfrac{1}{2}\rho h L V_r^2 C_l = 0, \tag{2}$$

where $m = m_b + m_a$, and m_b and m_a are the body mass and the added mass, respectively, and c is the viscous damping coefficient. The effective restoring force $k_r y$ is the sum of the

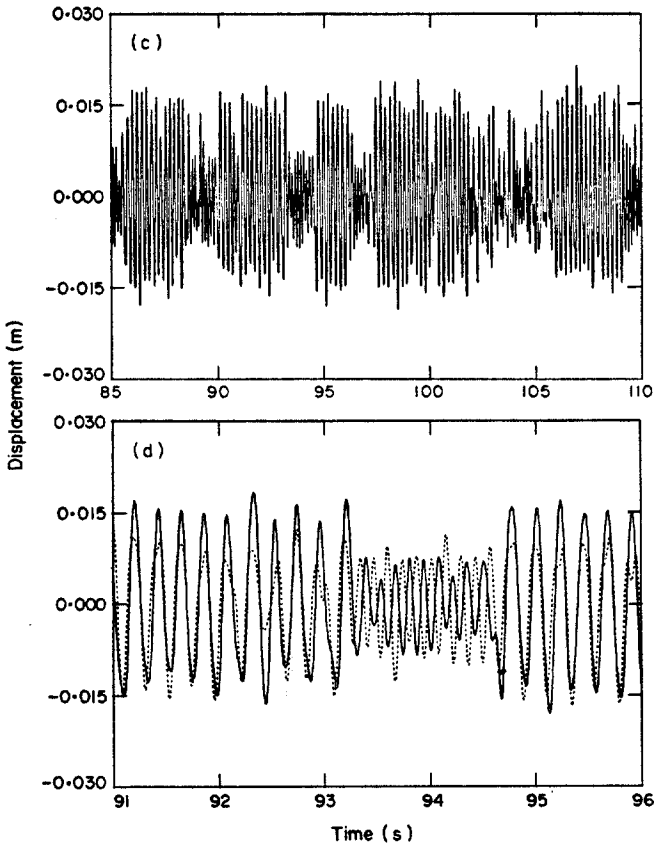

Figure 5—*continued.*

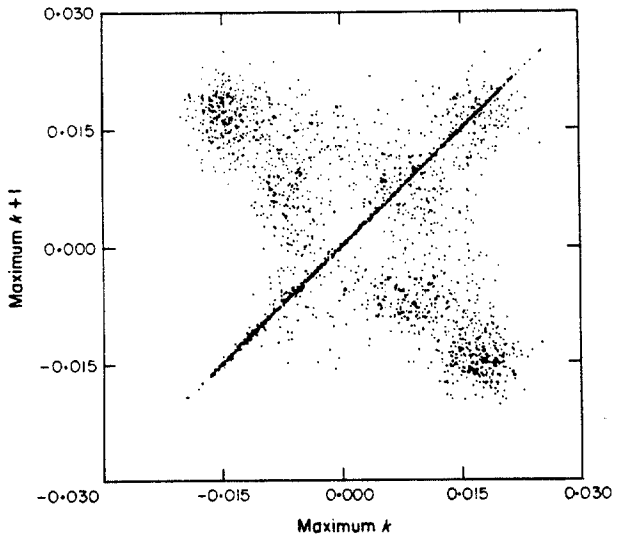

Figure 6. Poincaré plot, $V = 1{\cdot}77$ m/s.

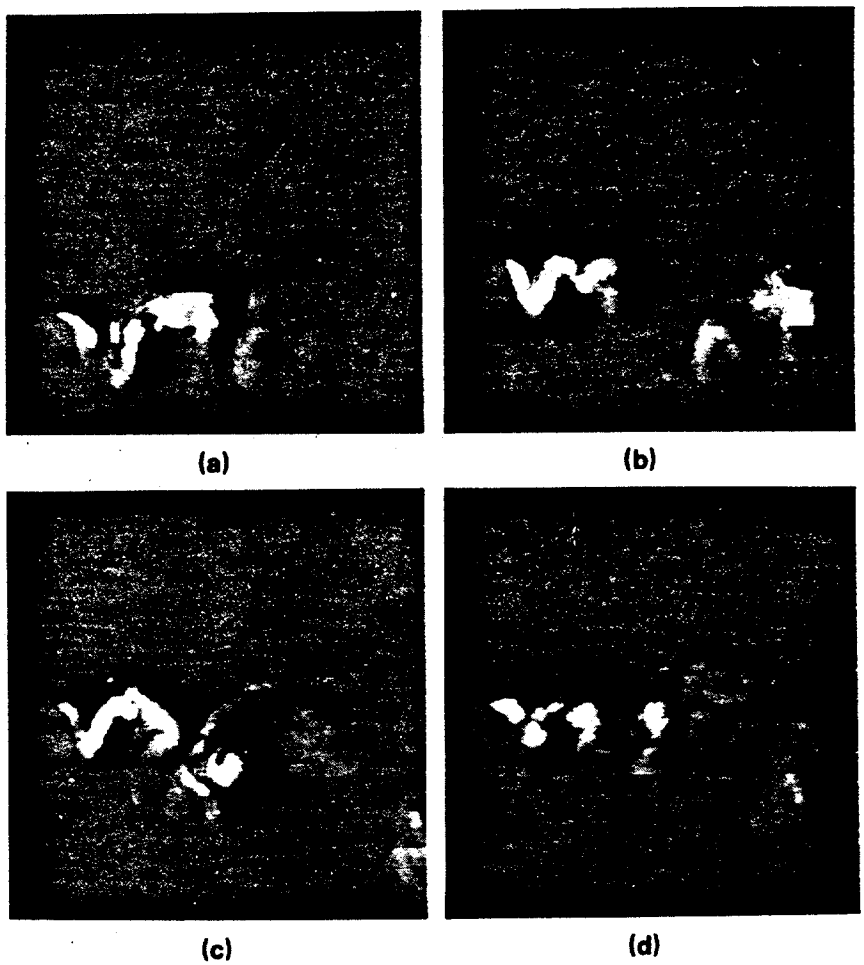

Figure 7. Flow visualization, top prism, double oscillator. Wakes at times: (a) 465/250 s; (b) 480/250 s; (c) 495/250 s; (d) 510/250 s.

spring restoring force and the vertical component of the tension in the drag wires:

$$k_r y = ky + \tfrac{1}{2}\rho C_D h L V_r^2 y/(r^2 - y^2)^{1/2}, \tag{3}$$

and V_r is the velocity of the flow relative to the prism, i.e., the sum of the mean flow velocity V and the absolute value of the horizontal component of the velocity of prism:

$$V_r = V + |y\dot{y}|/(r^2 - y^2)^{1/2}. \tag{4}$$

The second term in equation (4) is obtained by differentiating with respect to time the horizontal displacement of the oscillator due to the drag wire constraint,

$$x = r - (r^2 - y^2)^{1/2}. \tag{5}$$

It may be assumed that the drag coefficient $C_D = 2{\cdot}0$ (see, e.g., reference [16, p. 152]). Calculations showed that even relatively large deviations from that value (say, 30% or more) usually had no significant effects on the results. The fourth term on the left side of equation (2) is the drag force in the Morison equation for the threaded rods at the ends

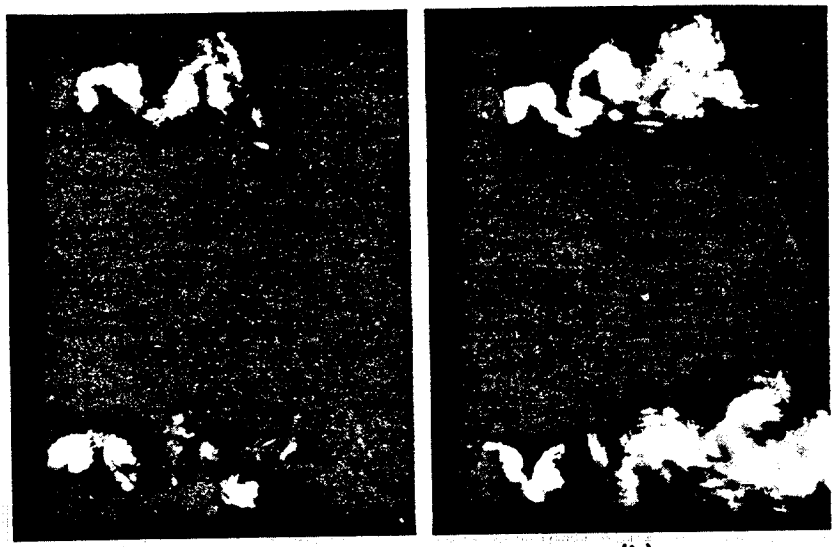

Figure 8. Wakes of top and of bottom prism: (a) vortex shedding of the two prisms occurring nearly in phase; (b) in nearly opposite phases.

of the prism and the drag wires; C_d is a Morison equation drag coefficient and A is the total projected area of the rods. C_t is the total lift force coefficient.

Using the notations $U=V/(\Omega h)$, $\Omega=(k/m)^{1/2}$, $\tau=\Omega t$, $2\beta=c/(m\Omega)$, $Y=y/h$, $N=\frac{1}{2}\rho h^2 L/m$, and dividing equation (2) through by kh, we obtain the non-dimensional form

$$Y''+2\beta Y'+[1+C_D N U_1^2 Y/(r^2/h^2-Y^2)^{1/2}]Y+NC_d(A/hL)Y'|Y'|-NU_1^2C_t=0, \quad (6)$$

$$U_1=U\{1+|YY'|/[U(r^2/h^2-Y^2)^{1/2}]\}. \quad (7)$$

Calculations showed that for our experiments the second term between brackets in equation (7) is typically in the range 0·01–0·05.

To define the equations of motion completely it is necessary to provide models for the added mass, the drag forces on the circular cylinders and the drag wires, and the total lift force coefficient C_t. These models are discussed in Appendices I and II.

5. NUMERICAL RESULTS FOR SINGLE OSCILLATOR

We first note that, with almost no exception, the results of the calculations were insensitive to changes within appropriate limits of the parameters β and C_d.

According to reference [10], the result of modeling the lift empirically for a single oscillator is that "some of the information about the system is lost". We present a few time histories, obtained numerically, that confirm this observation.

5.1. PARKINSON-SMITH MODEL WITH HARMONIC FORCING

We first show typical results obtained by using equations (2) and (A3). The phase space dimension in this case is three. It was shown in reference [23] that the behavior of a similar oscillator (with $A=0$ and $V_r\equiv V$) has similarities with the behavior of the standard circle map. Thus, if the forcing amplitudes exceed certain frequency-dependent critical values, chaotic motions may occur. Otherwise, the motions are periodic or quasi-periodic, and

are organized in accordance with the Arnold tongue pattern [4, 23–25]. The motion patterns are thus strictly controlled by the nature of equations (2) and (A3). For any given set of parameters it may therefore be expected that those patterns will be different from those inherent in the actual system, the phase space of which does not have three but infinitely many dimensions (or a finite but relatively large number of effective dimensions).

This is borne out by comparisons between Figures 3, 4 and their numerical counterparts, for which the parameters m_a and C_{vm} yielding the most satisfactory agreement with the observed motions were each arrived at after tens of trials and simulations. We show the numerical counterpart of Figure 3(a) in Figure 9(a) ($m=0{\cdot}23$ kg, $C_{vm}=1{\cdot}3$), and the counterpart of Figure 4(a) in Figure 10 ($m=0{\cdot}1$, $C_{vm}=0{\cdot}9$). Similar results were obtained for the numerical counterparts of Figure 3(b) ($m=0{\cdot}23$ kg, $C_{vm}=0{\cdot}3$) and Figure 4(b) ($m=0{\cdot}1$ kg, $C_{vm}=1{\cdot}3$), although in the latter case the amplitude modulation was smaller and the peak displacement slightly larger than for the observed motion.

The motion of Figure 9(a) is chaotic. This is suggested by the foldings of the Poincaré plot of Figure 9(b) (see, e.g., references [4 p. 93, 23, 24, 25 p. 178]), and is confirmed by the positive Lyapounov exponent ($l=2{\cdot}4$), calculated as in reference [25, p. 129] by following in time the difference between two solutions of the equations of motion, the initial conditions of which for y differ by, say, 0·1%. For $V=0{\cdot}90$ m/s the motion becomes quasi-periodic. We note in passing that in this and many other cases chaotic and quasi-periodic

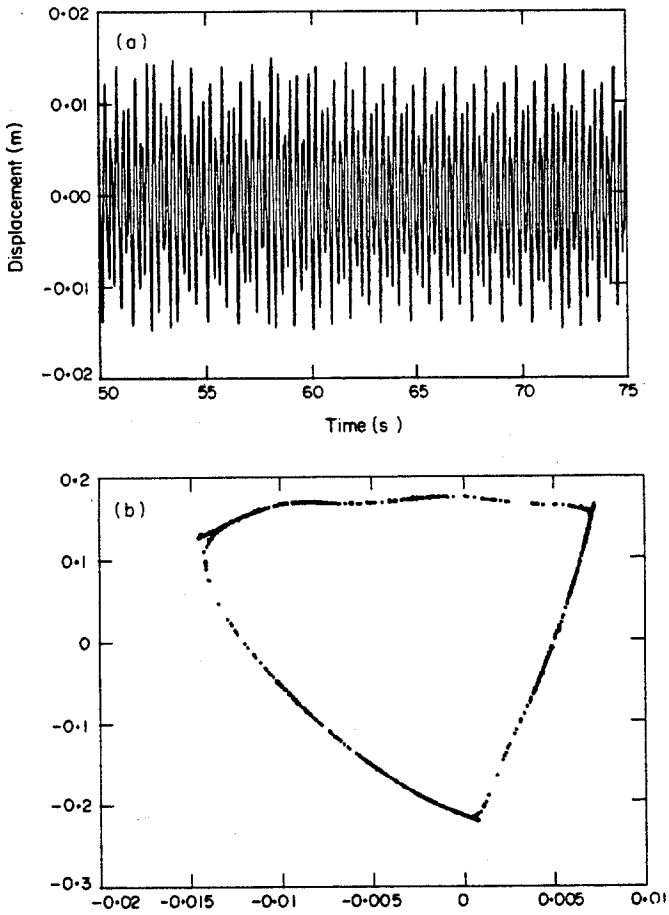

Figure 9. (a) Numerical simulation, single prism ($h=0{\cdot}0127$ m, aluminium), $V=0{\cdot}92$ m/s, harmonic lift model; (b) Poincaré plot corresponding to record partly shown in Figure 9(a).

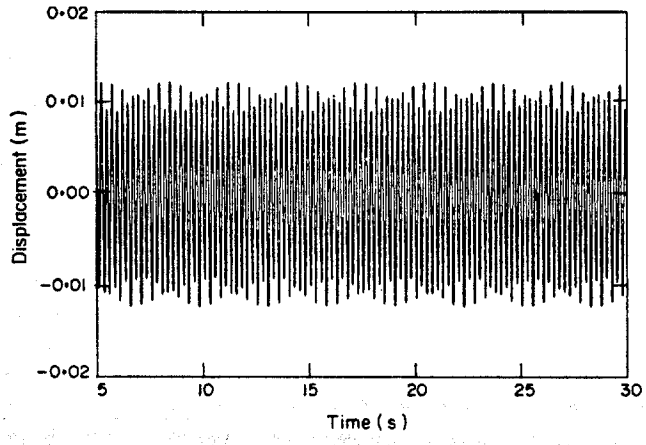

Figure 10. Numerical simulation, single prism ($h = 0{\cdot}00635$ m, steel), $V = 0{\cdot}91$ m/s, harmonic lift model.

motions are difficult to distinguish unless fairly elaborate tests are used. Thus, the fact that a motion is chaotic rather than, say, quasi-periodic is not necessarily in itself of significance from a structural engineering viewpoint.

5.2. PROPOSED LIFT OSCILLATOR

We now present a few typical results obtained by using equations (A4) and (A11) in conjunction with equation (2) and the assumption $\delta = 0$. This system has phase space dimension 4. The results show that, as for equations (2) and (A3), inherent in the system are oscillatory forms that can differ significantly from the observed ones, which are governed by the Navier–Stokes equations.

The counterpart to Figure 3(a), obtained by using $\varepsilon = 0{\cdot}2\ \text{s}^{-1}$, $m = 0{\cdot}22$ kg and initial conditions $y(0) = 0{\cdot}01$ m, $\dot{y}(0) = \dot{C}_v(0) = 0$, $C_v(0) = 0{\cdot}75$, yielded a response that was almost indistinguishable from Figure 9(a). Counterparts to Figure 3(b), obtained by using $\varepsilon = 0{\cdot}1\ \text{s}^{-1}$, $m = 0{\cdot}22$ kg, depended on the initial conditions being used. For $y(0) = 0{\cdot}01$, $\dot{y}(0) = \dot{C}_v(0) = 0$ and $C_v(0) = 1{\cdot}2$ (Figure 11(a)), there was no amplitude modulation; the frequency was higher than the observed value (3·7 Hz *vs.* 3·4 Hz); and the maximum peak was significantly lower than the observed value (0·033 m *vs.* 0·047 m). However, for $C_v(0) = 0{\cdot}3$ (Figure 11(b)), the opposite was true, i.e., the frequency was 3·25 Hz and the peak was 0·049 m. The numerical counterparts to Figure 4(a) ($V = 0{\cdot}91$ m/s) and Figure 4(b) ($V = 1{\cdot}77$ m/s) were similar to those obtained by using equations (2) and (A3). However, for $V = 1{\cdot}35$ m/s, regardless of the parameters m and ε and of the initial conditions being tried, no amplitude modulation could be obtained and the calculated steady state lift force associated with vortex shedding vanished, even though the amplitudes of the observed motion (not reproduced here) were strongly modulated. We also note that the use of parameters $\delta \neq 0$ in our proposed lift oscillator model did not improve the agreement between observations and numerical results.

We conclude that neither of the two models being tested here produces completely satisfactory simulations of the observed single oscillator motions. However, for some engineering purposes, the results may be viewed as acceptable first approximations.

6. EQUATIONS OF MOTION AND LIFT FORCE MODELS FOR DOUBLE OSCILLATOR

6.1. EQUATIONS OF MOTION

Let y_1 and y_2 denote the displacements of the top and bottom prism, respectively (Figure 1(b)). The notations for all parameters (except V) and other quantities pertaining to the

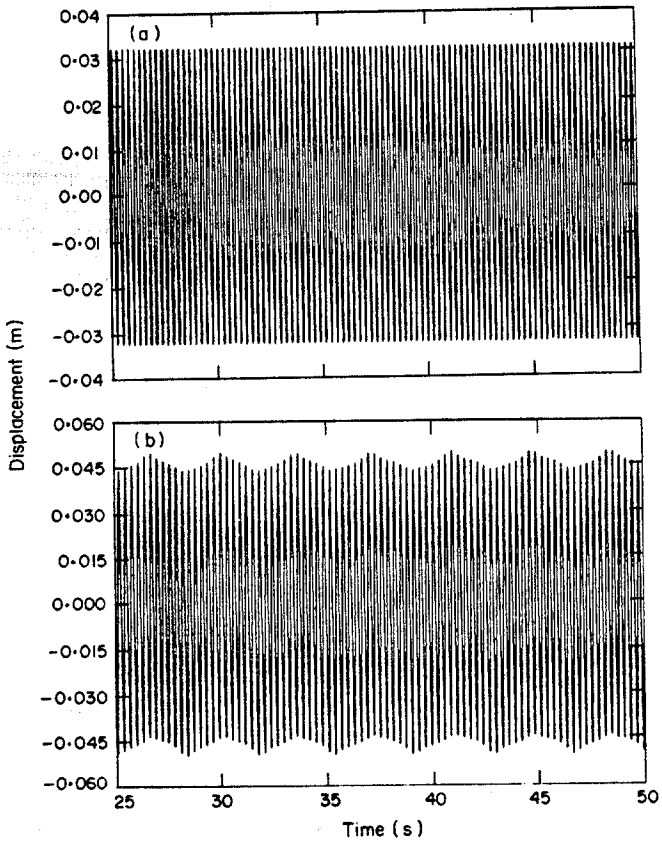

Figure 11. Numerical simulation, single prism ($h=0{\cdot}0127$ m, aluminium), lift oscillator model, $V=2{\cdot}62$ m/s: (a) $C_v(0)=1{\cdot}2$; (b) $C_v(0)=0{\cdot}3$.

uncoupled top and bottom oscillator are the same as for the single oscillator, except that they are affected by index 1 and 2, respectively. The corresponding equations of motion can be written as $D_1(y_1)=0$, $D_2(y_2)=0$, where the differential operators D_1 and D_2 are the same as the operator D of equation (2), except for the presence of the indices. The equations of motion for the double oscillator are then

$$D_1(y_1)+k_{12}(y_1-y_2)=0, \tag{8}$$

$$D_2(y_2)+k_{12}(y_2-y_1)=0. \tag{9}$$

Equations (8) and (9) may be non-dimensionalized in a manner similar to that used to obtain equation (6), for example by dividing through both equations by $K(h_1+h_2)/2$, where $K=(m_1+m_2)\Omega_1^2$.

$$\Omega_{1,2}=(1/2^{1/2})\{\sigma_1+\sigma_2\mp[(\sigma_1-\sigma_2)^2+4\sigma_3\sigma_4]^{1/2}\}^{1/2} \tag{10}$$

are the natural frequencies of the associated linear two-degree-of-freedom system and

$$\sigma_1=(k_1+d_{12})/m_1, \qquad \sigma_2=(k_2+k_{12})/m_2, \qquad \sigma_3=k_{12}/m_1, \qquad \sigma_4=k_{12}/m_2. \tag{11}$$

6.2. LIFT FORCES

The lift force models for each prism are similar to those used for the single oscillator. However, the observed vortex patterns (see Figure 8, where the vortex shedding on the

top and bottom prism occurs either in phase or in opposite phases) suggest that the fluid serves as an interaction agent between the lift forces acting on the two prisms. The form of the proposed lift oscillator equations (equation (A11), with the relevant terms affected by index 1 and 2, respectively) automatically ensures such interaction. However, one may add to those equations explicit lift force interaction terms $\phi_i(C_{v1}, C_{v2}, \dot{C}_{v1}, \dot{C}_{v2}, y_1, y_2, \dot{y}_1, \dot{y}_2)$, $i=1, 2$, respectively. For example, by analogy with the linear coupling model for the two mass oscillators, one could assume for the lift oscillators the simple coupling model

$$\phi_1 = -\gamma(2\pi n_{s1})^2 C_{v2}, \qquad \phi_2 = -\gamma(2\pi n_{s2})^2 C_{v1}, \tag{12}$$

where γ is a coupling constant; other interaction models could be attempted.

7. NUMERICAL RESULTS FOR DOUBLE OSCILLATOR

7.1. SIMPLE PARKINSON-SMITH MODEL

If the vortex-induced lift force is ignored the total lift force reduces to the simple Parkinson–Smith model given by equations (A1) and (A2) applied to each prism. It was found in reference [23] that, if this model is used, the numerical double oscillator is incapable of experiencing motions of the type shown in Figures 5(b, c). However, beyond a critical velocity V_{cs}, the attractor corresponding to the in-phase motions of the two prisms disappears, and the only remaining attractor, the domain of attraction of which is now the whole phase space, corresponds to out-of-phase motions of the two prisms. One may ask whether there is a correlation between the critical velocity V_{ce} beyond which motions of the type shown in Figures 5(b, c) occurred in the experiments (see Table 1)

TABLE 1

Spring constants for double oscillators and critical flow velocities V_{ce} and V_{cs}

Case (1)	Material (2)	h (mm) (3)	k_1 (N/m) (4)	k_{12} (N/m) (5)	k_2 (N/m) (6)	V_{ce} (m/s) (7)	V_{cs} (m/s) (8)
1	Aluminium	6·35	41	61	46	1·02	1·15
2			53	80	61	1·16	1·35
3			56	145	78	1·32	1·90
4	Steel	6·35	55	61	81	1·58	1·10
5			41	61	46	2·21	1·40
6			74	156	84	3·95	2·75

and the critical velocity V_{cs}. The latter was obtained from calculations in which the nominal added mass parameter was based on the expression of reference [26], without adjustments aimed at matching the calculated and the observed oscillation frequencies. The results showed that the ratio V_{cs}/V_{ce} depends on the non-dimensional parameters N_i $(i=1, 2)$, k_1/k_2 and k_1/k_{12}, and on the non-dimensionalized flow velocity, and that for the cases of Table 1, V_{ce} differed from V_{cs} by about 35% or less. The speed V_{cs} thus provides only a crude indication on the magnitude of V_{ce}.

7.2. PARKINSON-SMITH MODEL WITH HARMONIC FORCING

This model, which does not allow for flow–structure interaction, appeared to be incapable of yielding motions of the type shown in Figures 5(b, c).

7.3. PROPOSED LIFT OSCILLATOR MODEL

This model corresponds to an eight-dimensional phase space. We first report results obtained by assuming $\delta = \gamma = 0$. For the parameters corresponding to Figures 5(a, b), Figure 12(a) ($V = 0{\cdot}91$ m/s, $m_1 = 0{\cdot}065$ kg, $m_2 = 0{\cdot}063$ kg, $\varepsilon_1 = \varepsilon_2 = 0{\cdot}04$ s^{-1}) and Figure 12(b) ($V = 1{\cdot}34$ m/s, $m_1 = 0{\cdot}065$ kg, $m_2 = 0{\cdot}063$ kg, $\varepsilon_1 = \varepsilon_2 = 0{\cdot}065$ s^{-1}) show results of simulations for which the initial conditions were $y_i(0) = 0{\cdot}01$, $C_{vi}(0) = 1{\cdot}0$, $\dot{y}_i(0) = \dot{C}_{vi}(0) = 0$ ($i = 1, 2$).

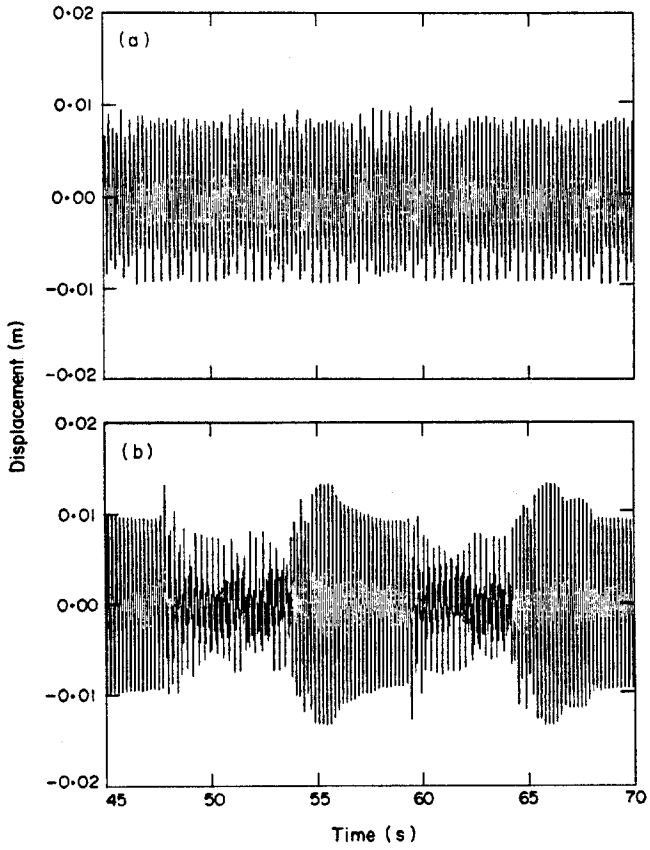

Figure 12. Numerical simulation, double oscillator, lift oscillator model ($h_1 = h_2 = 0{\cdot}00635$ m, aluminium prisms): (a) top prism, $V = 0{\cdot}91$ m/s; (b) top prism, $V = 1{\cdot}34$ m/s.

Note that both for $V = 0{\cdot}91$ m/s (Figure 12(a)) and for $V = 1{\cdot}34$ m/s (Figure 12(b)) the oscillation frequencies are higher for the simulated than for the observed records. In addition, for the record of Figure 12(b) alternations between the two oscillatory forms occur on the average at shorter intervals than in its observed counterpart (Figure 5(b)). The time history of Figure 12(b) is sensitive to initial conditions. This is seen in Figure 13, which shows the evolution with time of an initial separation between two time histories for which $y_2(0) = 0{\cdot}01$ m and $y_2(0) = 0{\cdot}0101$ m, respectively, all other initial conditions being the same (see reference [25, p. 129]). The average exponential growth of the initial separation, the irregular appearance of the time history, the spectral density plot (which was found to have significant broadband components), and the Poincaré plot (which is similar to Figure 6) suggest that for the parameters of Figure 12(b) our model may exhibit low-(eight-)dimensional chaotic behavior. If this were the case it would be permissible to

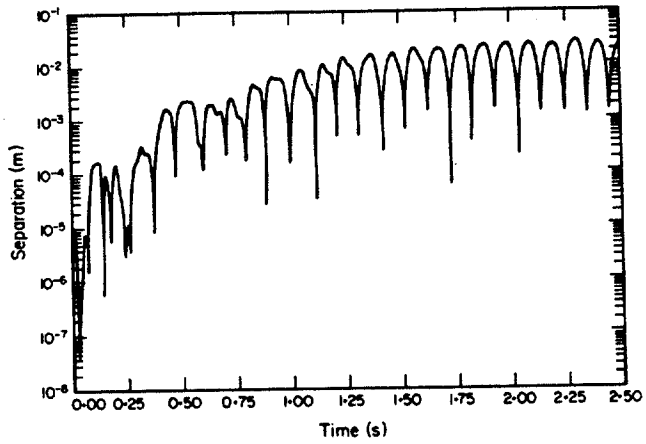

Figure 13. Growth of 0·0001 m initial separation with time, $V = 1{\cdot}34$ m/s.

assume that this may also be true of observed motions such as those of Figures 5(b, c), at least in some instances.

Time histories similar to those of Figure 12(b) were also obtained numerically by assuming that the lift oscillator coupling parameter $\gamma \neq 0$, e.g., for $V = 1{\cdot}77$ m/s, $m_1 = 0{\cdot}065$ kg, $m_2 = 0{\cdot}063$ kg, $\varepsilon_1 = \varepsilon_2 = 0{\cdot}5\ \text{s}^{-1}$, $\delta = 0$, $\gamma = 0{\cdot}8$, and the same initial conditions as for Figure 12. In this case also, the frequencies were higher than the corresponding experimental values (Figure 5(c)).

As for the single oscillator, by using parameter values $\delta \neq 0$ in the above lift oscillator model we were not able to obtain an improved agreement between calculated results and observations, either for $\gamma = 0$ or for $\gamma \neq 0$.

We conclude that, as in the case of the single oscillator, and despite the awesomely rich bifurcational structure of the system, the proposed model appears to be capable of yielding definitely imperfect but not altogether unreasonable approximate descriptions of observed motions. We note, however, that the range of parameters for which motions such as that of Figure 12(b) could be obtained appears to be extremely narrow.

8. SUMMARY AND CONCLUSIONS

In this paper we report typical results of experiments which confirm the finding, previously noted in reference [10], that hydroelastic single oscillator galloping generally exhibits significant amplitude modulation. The experiments revealed an interesting form of fluid-elastic behavior of the double oscillator, which occurs routinely if the flow speeds exceed certain values that depend upon the system parameters.

We review and assess existing empirical fluid-elastic models, and propose an alternative empirical model which incorporates information on the dependence of the Strouhal number and the vortex-induced lift coefficient on angle of attack. We show typical results of numerical calculations aimed at assessing the usefulness of those models. The results suggest that, despite the unavoidable uncertainties concerning the form of the equation of motion and the actual parameter values, these models appear to be capable of providing a definitely imperfect, but by and large not unreasonable, description of observed motions of the single oscillator. However, there are pitfalls, since inherent in the structure of the low-dimensional empirical system of differential equations being used are periodicities and multiple solutions that may not be representative of the behavior of the Navier–Stokes

equations for the actual system. In particular, it was found that this may lead to predictions that underestimate the response.

In the case of the double oscillator we found that our proposed lift oscillator model, which corresponds to a system with an eight-dimensional phase space, also appears to be capable of describing observed motions (including apparently chaotic behavior), at least to a first approximation. However, the windows corresponding to such behavior tend to be quite narrow, i.e., for such behavior to occur the values of the adjustable parameters must be within a very narrow range. For this reason empirical models available so far, including ours, cannot predict reliably motions such as those of Figure 5(b, c). (Poor predictive capabilities have also been noted, although not explained, for chaotic fluid-elastic motions of a streamlined body [27].)

The shortcomings of empirical fluid-elastic models such as those reviewed or proposed in this paper are not surprising. Empirical models are constructed by piecing together disparate pieces of information characterizing certain aspects of fluid-dynamic and fluid-elastic behavior. This is done within the framework of a partly arbitrary system of differential equations that includes a deliberately simple (van der Pol) non-linear lift oscillator equation. Our results suggest that this degree of arbitrariness and the fragmentary information used to construct such empirical models can lead to significant differences of structure between those models on the one hand and the Navier–Stokes equations governing the actual system on the other. These differences may lead to failure to predict certain types of behavior.

The apparently chaotic behavior revealed by our experiments thus appears to be an example of undesirable fluid-elastic oscillation that can easily be missed by conventional empirical fluid-elastic models. From the viewpoint of structural reliability, this is more serious than predicting undesirable fluid-elastic behavior; as was done, e.g., in references [1, 2], when in fact according to experiments none appears to exist.

The mixed performance of conventional empirical models does not exclude the possibility of developing on their basis more satisfying tools for detecting fluid-elastic chaos or similar dynamic behavior. A phenomenon that was not accounted for in this paper is that small flow fluctuations, including fluctuations associated with the three-dimensionality of the flow, induce random forces on the prisms. In some instances the effect of the fluctuations may be unimportant. However, under certain circumstances these forces may drive the orbit intermittently from one attractor to the other ("basin hopping"; see, e.g., reference [28]). Other noise-induced mechanisms could be at work, both for the observed motions [29, 35–37] and for simulated motions such as those of Figure 12(b) (for which the chaotic behavior could be induced by numerical noise [38].) One possible approach to modeling motions such as those of Figure 5(b, c) would be to develop a non-autonomous system by applying to the empirical fluid-elastic equations suitable random excitations, the nature and magnitude of which might be obtainable in part from systematic measurements of lift forces, such as were attempted in reference [30]. It may be expected that such an approach could increase the size of the parameter windows to which there corresponds apparently chaotic behavior, and thus improve the predictive capability of empirical fluid-elastic models. The potential of this approach appears to be worth exploring given the current absence of practical alternatives to modeling bluff body fluid-elastic behavior.

ACKNOWLEDGMENTS

We wish to thank the following David Taylor Research Center staff: Dr T. T. Huang, for permission to use the water tunnel and his kind support; S. Gowing and G. Baglin, for their effective collaboration; P. Congedo for the photographic and videotaping work;

and S. McGuigan for the flow visualization. Thanks are also due to Professor R. H. Scanlan of Johns Hopkins University, to Dr H. A. Fowler of the Computing and Applied Mathematics Laboratory, NIST, and Dr R. D. Marshall of the Building and Fire Research Laboratory, NIST, for their critical comments on the original manuscript. Dr R. D. Marshall also provided invaluable advice and assistance in the experimental phase of the work. The assistance of F. Rankin, Dr N. Carino and E. Anderson, of the Building and Fire Research Laboratory, NIST is also acknowledged with thanks.

REFERENCES

1. R. C. T. RAINEY 1977 *Paper No. 6, Proceedings, The Royal Institute of Naval Architects*, 59–80. The dynamics of tethered platforms.
2. J. R. PAULLING 1982 *Proceedings, Ocean Structural Dynamics Symposium* '82, 586–603. Mathieu Instabilities in TLP response.
3. J. M. T. THOMPSON, A. R. BOKAIAN and R. GHAFFARI 1984 *ASME Journal of Energy Resources Technology* **106**, 191–198. Subharmonic and chaotic motions of compliant offshore structures and articulated mooring towers.
4. J. M. T. THOMPSON and H. B. STEWART 1987 *Nonlinear Dynamics and Chaos*. Chichester: John Wiley.
5. S. KATO and S. OHMATSU 1989 *Eighth International Conference on Offshore Mechanics and Arctic Engineering, The Hague*. Hydrodynamic forces and pressure distributions on a vertical cylinder oscillating in low frequencies.
6. C. Y. LIAW 1989 *Eighth International Conference on Offshore Mechanics and Arctic Engineering, The Hague*. Complex dynamics of a simple cylinder in regular waves.
7. E. H. DOWELL 1982 *Journal of Sound and Vibration* **85**, 333–344. Flutter of a buckled plate as an example of chaotic motion of a deterministic autonomous system.
8. M. P. PAÏDOUSSIS, G. X. LI and F. C. MOON 1989 *Journal of Sound and Vibration* **135**, 1–19. Chaotic oscillations of the autonomous system of a constrained pipe conveying fluid.
9. G. V. PARKINSON and J. D. SMITH 1964 *Quarterly Journal of Mechanics and Applied Mathematics* **17**, 225–239. The square prism as an aeroelastic nonlinear oscillator.
10. G. V. PARKINSON and D. BOUCLIN 1977 *Safety of Structures under Dynamic Loading* (I. Holand *et al.*, editors), 737–742. Norwegian Institute of Technology Trondheim. Hydroelastic oscillations of square cylinders.
11. G. V. PARKINSON 1980 *Practical Experiences with Flow-induced Vibrations* (E. Naudascher and D. Rockwell, editors), 786–797. Berlin: Springer. Nonlinear oscillator modelling of flow-induced vibrations.
12. T. SARPKAYA and M. ISAACSON 1981 *Mechanics of Wave Forces on Offshore Structures*. New York: Van Nostrand Reinhold.
13. E. H. DOWELL 1981 *Journal of Sound and Vibration* **75**, 251–264. Non-linear oscillator models in bluff body aeroelasticity.
14. R. T. HARTLEN and I. G. CURRIE 1970 *Proceedings of the American Society of Civil Engineers* **EM5**, 577–591. Lift oscillator model of vortex-induced vibration.
15. K. Y. R. BILLAH 1989 *Ph.D. Dissertation, Department of Civil Engineering, Princeton University*. A study of vortex-induced vibration.
16. E. SIMIU and R. H. SCANLAN 1986 *Wind Effects on Structures* (second edition). New York: John Wiley.
17. E. H. DOWELL, H. C. CURTISS, R. H. SCANLAN and F. SISTO 1989 *A Modern Course in Aeroelasticity* (second revised and enlarged edition). Dordrecht: Kluwer.
18. F. C. MOON 1987 *Chaotic Vibrations*. New York: John Wiley.
19. F. C. MOON and G. X. LI 1990 *American Institute of Aeronautics and Astronautics Journal* **28**, 915–921. Experimental study of chaotic vibrations in a pin-jointed space truss structure.
20. L. GLASS and P. HUNTER 1990 *Physica D* **43**, 1–16. There is a theory of heart.
21. F. C. MOON and P. J. HOLMES 1979 *Journal of Sound and Vibration* **65**, 285–296. A magneto-elastic strange attractor.
22. G. R. COOK and E. SIMIU 1991 *Journal of Engineering Mechanics* **117**, 2049–2064. Periodic and chaotic oscillations of modified Stoker column.

over the length of the wires the vertical velocity varies approximately linearly with distance from their fixed point. We assume an average value C_{dw} of the drag coefficient, to be used throughout the length of the wires. The drag force associated with the Morison equation for the two wires may be established by integration along the length of the wires. This yields a total wire drag force $D_w = 2 \times \frac{1}{2}\rho d_w r C_{dw} \dot{y}|\dot{y}|/3$. For the two threaded rods at the ends of the square prism the drag force is $D_c = 2 \times \frac{1}{2}\rho d_c L_c C_{dc} \dot{y}|\dot{y}|$. The fourth term in equation (6) represents the sum of these two forces provided that C_d and A are chosen appropriately. We used $A = 2 \times r \times d_w/3 + 2 \times L_c \times d_c = 2 \times 400 \times 0{\cdot}328/3 + 2 \times 60 \times 2 = 330\ \text{mm}^2$, and various values of C_d within the range suggested earlier. As pointed out in reference [10], hydrodynamic galloping calculations are not affected significantly by even relatively large uncertainties in the viscous mechanical dissipation. This was confirmed by numerous calculations performed for various values $0{\cdot}3 < C_d < 2{\cdot}0$ and $0{\cdot}01 < \beta < 0{\cdot}02$.

APPENDIX II: MODELING OF LIFT FORCES

Since the oscillation amplitudes that we are concerned with are large ($y/h > 1$ or so), the along-span correlation of the fluid-elastic forces may be assumed to be close to unity [16, p. 201]. The fact that, for the double oscillator, the flow adjusts to the oscillations so that the vortex shedding of the two prisms is strongly coherent (Figure 8) lends additional support to this assumption.

AII.1. REVIEW OF LIFT FORCE MODELS FOR SINGLE OSCILLATOR

In this section lift force models proposed in the literature are reviewed and discussed. An alternative model is then presented.

Simple Parkinson–Smith model. Galloping experiments in air (i.e., for small values of NU^2) were reported in reference [9] for Reynolds numbers $4000 \leqslant Re \leqslant 36\,000$, with no drag wires and no connecting circular cylinders projecting from the prisms' ends (i.e., $A = 0$, $V_r \equiv V$ and $k_r \equiv k$). For ratios of vortex shedding frequency to oscillation frequency, n_s/n_o, appreciably greater than unity (a restriction that also pertains to this study), the results of those experiments were shown to be consistent with the assumption that the lift force is

$$C_l \equiv C_L, \tag{A1}$$

$$C_L = a_1 \dot{y}/V_r - b_1(\dot{y}/V_r)^3 + c_1(\dot{y}/V_r)^5 - d_1(\dot{y}/V_r)^7, \tag{A2}$$

where $a_1 = 2{\cdot}69$, $b_1 = 168$, $c_1 = 6270$, $d_1 = 59\,900$. Unless $c \geqslant a_1 V_r$, the solutions of equations (2) and (A1) corresponding to any given set of initial conditions are periodic and exhibit no amplitude modulation.

Parkinson–Smith model with harmonic forces. For relatively large NU^2 (typically for oscillations in water as opposed to air), the experiments of reference [10] as well as ours showed that equation (A1) is inadequate. Indeed, our calculations showed that equation (A1) could not account for the observed amplitude modulations.

Assuming $S = 0{\cdot}125$ [31, 32], for Figure 3(c), equation (1) yields $n_s \simeq 9{\cdot}1$ Hz, whereas $n_o = 3{\cdot}4$ Hz. In this case the ratio $n_s/n_o = 2{\cdot}7$. This ratio is considerably larger in all other cases. The inadequacy of the Parkinson–Smith model is thus not attributable to small ratios n_s/n_o. Nor is it attributable to differences in Reynolds numbers ($Re = 10^6 Vh$), since for Figure 3 these vary between 5800 and 33 300, i.e., well within the range covered by the measurements of reference [9]. Therefore, to account for the amplitude modulations, alternative models are required. These should reflect the effect of the excitation due to

23. E. SIMIU and G. R. COOK 1991 *Journal of Engineering Mechanics* **117**, 241–259. Chaotic motions of self-excited forced and autonomous square prisms.
24. J. A. GLAZIER and A. LIEBCHABER 1988 *IEEE Transactions on Circuits and Systems* **25**, 790–809. Quasi-periodicity and dynamical systems: an experimentalist's view.
25. P. BERGÉ, Y. POMEAU and C. VIDAL 1986 *Order Within Chaos*. New York: John Wiley.
26. J. N. NEWMAN 1980 *Marine Hydrodynamics*. Cambridge, Massachusetts: The M.I.T. Press.
27. A. J. HAUENSTEIN, R. M. LAURENSON, W. EVERSMAN, G. GALECKI, I. QUMEI and A. A. AMOS 1990 *Paper AIAA-90-1034-CP, American Institute of Aeronautics and Astronautics*, 1530–1539. Chaotic response of aerosurfaces with structural nonlinearities.
28. F. T. ARECCHI, R. BADII and A. POLITI 1985 *Physical Review A* **32**, 402–408. Generalized multistability and noise-induced jumps in a nonlinear dynamical system.
29. E. STONE and P. HOLMES 1990 *SIAM Journal on Applied Mathematics* **50**, 726–743. Random perturbations of heteroclinic attractors.
30. Y. OTSUKI, K. WASHIZU, H. TOMIZAWA and A. OHYA 1973 *Journal of Sound and Vibration* **34**, 233–248. A note on the aeroelastic stability of a prismatic bar with a square section.
31. B. J. VICKERY 1966 *Journal of Fluid Mechanics* **25**, 481–494. Fluctuating lift and drag on a long cylinder of square cross-section in a smooth and in a turbulent stream.
32. Y. NAKAMURA and T. MIZOTA 1975 *Journal of the ASCE Engineering Mechanics Division* **101**, 855–871. Unsteady lifts and wakes of oscillating rectangular prisms.
33. J. J. STOKER 1950 *Nonlinear Vibrations*. New York: Interscience.
34. E. J. CUI and E. H. DOWELL 1981 *Advances in Aerospace Structures and Materials, ASME Winter Annual Meeting*, 155–173. An approximate method for calculating the vortex-induced oscillation of bluff bodies in air and water.
35. N. AUBRY, P. HOLMES, J. L. LUMLEY and E. STONE 1988 *Journal of Fluid Mechanics* **192**, 115–173. The dynamics of coherent structures in the wall region of a turbulent boundary layer.
36. E. STONE 1990 *Physics Letters A* **148**, 434–442. Power spectra of the stochastically forced Duffing oscillator.
37. T. KAPITANIAK 1988 *Chaos in Systems with Noise*. Singapore: World Scientific.
38. M. J. ABLOWITZ and B. M. HERBST 1990 *SIAM Journal on Applied Mathematics* **50**, 339–351. On homoclinic structure and numerically induced chaos for the nonlinear Schrodinger equation.

APPENDIX I: MODELING OF ADDED MASS, AND OF DRAG FORCES ON ANCILLARY PARTS

AI.1. BODY AND ADDED MASS

The total body mass m_b includes the mass of the prism and its appurtenances, and the tributary mass of the springs attached to it. The added mass m_a includes the added mass for the prism and the inertial term in the Morison equation for the threaded rods and the drag wires. Assuming that the added mass coefficient for circular cylinders is of the order of unity, this Morison inertial term is of the order of $\rho[(2\times 0{\cdot}4\times 0{\cdot}000328^2\times 0{\cdot}785)/2+2\times 0{\cdot}06\times 0{\cdot}002^2\times 0{\cdot}785]\ \ddot{y}=\rho\times 3{\cdot}8\times 10^{-6}\ddot{y}$. (The factor $\frac{1}{2}$ in the first term of the square bracket is the result of averaging the vertical acceleration over the length of the wires assumed to be straight.) In still fluid the added mass term for a square prism is $1{\cdot}1885\rho h^2L\ddot{y}$ [26, p. 145]. If we used this value the total added mass effect would be $m_a\ddot{y}=\rho h^2L\ddot{y}(1{\cdot}1885+3{\cdot}8\times 10^{-6}/h^2L)$. We would thus have $m_a\simeq 0{\cdot}015$ kg for the 6·35 mm prisms, and $m_a\simeq 0{\cdot}045$ kg for the 12·7 mm prisms. However, as was observed in reference [10], the use of added mass corresponding to still water conditions can lead to a significant underestimation of the oscillation frequencies. This was confirmed by our results. The added mass must therefore be determined empirically to match the observed oscillation frequencies.

AI.2. DRAG FORCES ON CIRCULAR CYLINDERS AND DRAG WIRES

There appears to be little information on the coefficient C_d (see equation (2)) for body oscillations in the presence of a relatively large mean speed. Extrapolations from available data suggest that $0{\cdot}3\leqslant C_d\leqslant 2{\cdot}0$ is a reasonable assumption [12]. Observations showed that

vortex shedding. For example, since the vortex shedding appears to be nearly periodic with the period given by equation (1), it may be assumed that, approximately,

$$C_l = C_L + C_{vm} \cos(2\pi n_s t). \tag{A3}$$

(Or, using equation (1), $C_l = C_L + C_{vm} \cos(2\pi US\tau)$.) We refer to equation (A3) as the Parkinson–Smith model with added harmonic forcing. To attempt to match the calculated and observed motions, appropriate values must be tried for the parameters m_a and C_{vm}. Alternatively, if the appropriate information were available, the second term on the right side of equation (A3) could be replaced by a sum of terms, possibly with phase angles obtained by Monte Carlo simulation, to account for the fact that the spectral density of the lift associated with vortex excitation has a finite bandwidth.

Equation (A3) does not allow for flow–structure interaction since C_{vm} is constant. It is nevertheless useful for suggesting that, as was done in reference [9], the vortex shedding excitation may be neglected if NU^2 is small. Indeed, according to calculations based on equations (2) and (A3), for the parameter ranges of reference [9] the effect on the motion of using equation (A3) instead of equation (A1) is imperceptible. This is true even if the values assumed for C_{vm} are unrealistically large (e.g., up to $C_{vm} = 6{\cdot}0$).

Parkinson–Bouclin model. A model in which the structure and the fluid interact was proposed in reference [10], which adapted to the case of the oscillating square prism a lift oscillator model of the Hartlen–Currie type as follows:

$$C_l = C_L + C_v, \tag{A4}$$

where C_v satisfies the equation:

$$\ddot{C}_v + (\text{non-linear term in } \dot{C}_v) + (2\pi n_s)^2 C_v - f(\dot{y}) = 0, \tag{A5}$$

and the non-linear term and $f(\dot{y})$ are so chosen that, for $\dot{y} = 0$, C_v has frequency n_s and amplitude C_{v0} equal to the mean vortex excitation lift coefficient for the stationary body. (We note that in reference [10], n_s and C_{v0} are assumed to be independent of the angle of attack.) A non-linear term that meets these requirements is

$$\varepsilon(-\dot{C}_v + a\dot{C}_v^3), \tag{A6}$$

where [33, pp. 128, 134]

$$a = (4/3)/(2\pi n_s C_{v0})^2. \tag{A7}$$

The term $f(\dot{y})$ is included for the purpose of coupling equations (2) and (A5). For simplicity it was assumed in reference [10] that $f(\dot{y}) = \delta\dot{y}$, although other choices are possible [11]. The constants δ and ε (as well as m_a) are chosen by trial and error. Equation (A6) may be non-dimensionalized by using $\tau = \Omega t$ and then dividing the equation through by Ω^2. The term given by equation (A6) then becomes $\varepsilon/\Omega(C_v' + a\Omega^2 C_v'^3)$, and the term δy becomes $(\delta h/\Omega)Y'$.

Dowell model. A similar model, developed for circular cylinders, was proposed in reference [13], where it was assumed that C_l is the solution of the lift oscillator equation

$$\ddot{C}_l + (\text{non-linear term in } \dot{C}_l) + (2\pi n_s)^2 C_l + B_1(h/V^2)\dddot{y} + (2\pi n_s)^2 C_L = 0, \tag{A8}$$

where B_1 is an added mass coefficient, and the non-linear term has a form similar to that of (or can have the same form as) equation (A6). Thus, for $\dot{y} \equiv 0$, C_l has frequency n_s and amplitude C_{v0}. The added mass effect is introduced through the term in $\dddot{y}$. The primary motivation in reference [13] was to achieve a physically consistent model, in which the coupling of equations (2) and (A8) occurs naturally through the terms in $\dot{y}$ and $\dddot{y}$ of

equation (A8), so that no arbitrary coupling term is needed. This model was tested successfully for circular cylinders in references [13, 34]. However, calculations showed that for square cylinders the model needed to be modified.

AII.2. PROPOSED LIFT OSCILLATOR MODEL

Following Dowell, we seek a model in which the coupling between equation (2) and the equation defining C_v is natural. This can be accomplished if it is noted that for the stationary square prism both the vortex-induced lift coefficient and the Strouhal number depend upon the angle of attack $\dot{y}/V_r$ [31, pp. 484, 486]. For the interval $\dot{y}/V_r$ of interest in galloping problems ($0 \leqslant \dot{y}/V_r \leqslant 0{\cdot}3$), the data of reference [31] are approximately consistent with the expressions

$$S(y, \dot{y}) = S_0 + S_1 \sin \{S_2[S_3 + \dot{y}/V_r(y, \dot{y})]\}, \tag{A9}$$

$$C_{v0}(y, \dot{y}) = c_0 + c_1 \sin \{c_2[c_3 - \dot{y}/V_r(y, \dot{y})]\}, \tag{A10}$$

where the constants S_j and c_j ($j = 0, 1, \ldots, 3$) depend on the turbulence intensity i; for $i = 0{\cdot}02$, it follows from the data of reference [31] that $S_0 \simeq 0{\cdot}125$, $S_1 \simeq 0{\cdot}005$, $S_2 \simeq 8{\cdot}976$, $S_3 \simeq -0{\cdot}175$ and $c_0 \simeq 0{\cdot}925$, $c_1 \simeq 0{\cdot}475$, $c_2 \simeq 11{\cdot}2$, $c_3 \simeq 0{\cdot}14$. Within a cycle, the largest deviations of S from its average value are about $\pm 5\%$.

Our proposed lift model consists of equation (11) in which C_v satisfies equation (A11):

$$\ddot{C}_v + \varepsilon\{-\dot{C}_v + (4/3)/[2\pi S(y, \dot{y}) V_r(y, \dot{y}) C_{v0}(y, \dot{y})/h]^2 \dot{C}_v^3\} + (2\pi n_s)^2 C_v - \delta\dot{y} = 0. \tag{A11}$$

Since the presence of the variables y and $\dot{y}$ in equation (18) assures coupling with equation (2) (via equations (A9), (A10)), we may assume that $\delta = 0$, thus discarding the arbitrary factor δ in favor of realistic physical information on the behavior of the prism at rest. The parameters that must be selected by the analyst are then m_a and ε. The proposed model differs from the Parkinson–Bouclin model insofar as it incorporates the dependence on angle of attack of the vortex-induced lift coefficient and Strouhal number for the stationary prism.

The phase space dimension for the proposed lift oscillator model is four, whereas for the actual oscillator it is infinity. One could in principle write C_v as follows:

$$C_v = \sum C_{vi}, \tag{A12}$$

($i = 1, 2, \ldots, n$), where C_{vi} would be defined by equations similar to the equation for C_v in the preceding model, except that in these equations the lift coefficients and the frequencies would correspond to the ordinates and frequencies of the spectral density of the lift due to vortex shedding, and randomly selected phase angles would be added to the arguments of C_{vi}. This would increase the dimension of the phase space to $4(i+1)$.

APPENDIX III: NOMENCLATURE

A	projected area of threaded rods
B_1	added mass coefficient in equation (A8)
$\dot{c}$	damping coefficient
c_0, c_1, c_2, c_3	constants in equation (A10)
C_d, C_{dc}, C_{dw}	overall drag coefficient in Morison equation, drag coefficient for threaded rod, for wire, respectively
C_D	drag coefficient for square prism (equation (3))
C_L	galloping (self-excited) lift coefficient (equation (A2))
C_t	total lift coefficient (equations (2, A1, A3, A4))

C_v, C_{vi}, C_{v0}	lift coefficient associated with vortex shedding excitation, lift coefficients in equation (A12), lift coefficient for prism at rest, respectively
C_{vm}	lift coefficient in harmonic lift model (equation (A3))
d_c, d_w	diameter of threaded rod attached to prism end, and of drag wire, respectively
D, D_1, D_2	differential operator for single oscillator (equation (2)), for top prism, and for bottom prism, respectively
D_c, D_w	drag force on threaded rod attached to prism end, and on wire, respectively
h	width of prism
k	total stiffness of single oscillator springs
k_r	effective stiffness (equation (3))
k_1	stiffness of top spring
k_2	stiffness of bottom spring
k_{12}	stiffness of coupling spring
l	Lyapounov exponent
L	length of prism
L_c	clear length of circular cylinder at prism end
m, m_1, m_2, m_a	total mass of single oscillator, of top oscillator, of bottom oscillator, and added mass, respectively
m_c, m_l, m_u	mass of top, coupling, and bottom spring, respectively
n_o, n_s	oscillation frequency, and vortex shedding frequency, respectively
N	non-dimensional parameter in equation (6)
r	length of drag wire
S, S_0, S_1, S_2, S_3	Strouhal number, constants in equation (A9)
U, U_1	non-dimensional velocity, and effective non-dimensional velocity (equation (6))
V, V_{ce}, V_{cs}, V_r	flow velocity, critical flow velocity beyond which lively chaos occurs in actual system, critical flow velocity for which one attractor vanishes in simplified numerical model, and effective flow velocity (equation (4)), respectively
x	horizontal displacement
y, y_1, y_2, Y	vertical displacement of single, of top, and of bottom oscillator, and non-dimensional vertical displacement, respectively
α	quantity defined by equation (A7)
β	ratio of damping to critical damping
γ	lift oscillator coupling parameter
δ	constant
ε, ε_1, ε_2	parameter in equation (A6) applicable to single oscillator, to top oscillator, to bottom oscillator
ρ	fluid specific mass
σ_i	parameters defined by equation (11)
Ω, $\Omega_{1,2}$	$(k/m)^{1/2}$, circular frequencies given by equation (10)